

EIGHTEENTH EUROPEAN ROTORCRAFT FORUM

B - 05

Paper No 62

**EXPERIMENTAL AND COMPUTATIONAL INVESTIGATION OF A
CIRCULATION CONTROLLED TAIL BOOM**

**A NURICK, C GROESBEEK
UNIVERSITY OF THE WITWATERSRAND
SOUTH AFRICA**

**September 15-18, 1992
AVIGNON, FRANCE**

ASSOCIATION AERONAUTIQUE ET ASTRONAUTIQUE DE FRANCE

EXPERIMENTAL AND COMPUTATIONAL ANALYSIS OF A HELICOPTER CIRCULATION CONTROLLED TAIL BOOM

Alan Nurick and Cornelis Groesbeek
Branch of Aeronautical Engineering
University of the Witwatersrand, Johannesburg

ABSTRACT

The flowfield and torque characteristics of a circulation controlled helicopter tail boom about the main rotor axis of a hovering rotor were investigated experimentally and computationally. Empirical relationships between the boom torque, rotor torque and thrust and circulation air pressure are developed from the experimental results for the geometry considered. The limiting cases of tail boom torque due to the circulation control air in the absence of rotor downwash and the effects of the rotor torque in the absence of circulation control air, on the boom torque are included. The flowfield on the tail boom, without rotor downwash is analysed using a 2D Navier-Stokes code. Turbulent eddy viscosity is modelled in regions close to the surface of the tail boom using van Driest's method and in other areas by means of a k - ϵ model. Good correlation was obtained between the experimental and computationally derived velocity profiles in the boundary layer, its point of separation and the torque developed by the tail boom when the constants for the k - ϵ model were adjusted slightly.

NOTATION

- C_{μ} = slot momentum coefficient = $\rho V_f^2 t / \rho U_{\infty}^2 R_b$
 H = distance between rotor disc plane and tail boom centre line
 i, j = coordinate indices
 k = turbulent kinetic energy
 L = length along tail boom
 l_m = mixing length
 P = static pressure of air in the tail boom
 R_b = tail boom radius
 R_r = rotor radius
 t = slot thickness
 y, δ = distance from boom surface
 y^+ = $y V_* / \nu$
 Q = tail boom torque
 Q_r = rotor torque
 V_* = $\sqrt{\tau / \rho}$ = friction velocity
 ρ = air density
 μ = kinematic viscosity of air
 U = velocity vector
 ϵ = isotropic dissipation function
 ϕ = $2 \epsilon_{ij} \epsilon_{ij}$: Viscous dissipation is $\mu \phi$
 τ = wall shear stress
 ϵ_{ij} = $\frac{1}{2} (U_{i,j} + U_{j,i})$
 κ = von Karman Constant

1. INTRODUCTION

Hughes Helicopters Inc [1,2] initiated a programme to replace the tail rotor of a conventional helicopter used to balance the torque applied to the main rotor with a system comprised of a circulation controlled tail boom, a thruster installed at the aft end of the tail boom and vertical aerodynamic surfaces. The system has been developed and implemented by McDonnell Douglas Helicopter Company. Recognising the advantages of the circulation controlled tail boom and the opportunities for research of the complex flowfield a research programme was instituted at the University of the Witwatersrand. Some of the results obtained in this programme are presented.

The attachment of a jet to a convex surface was described by Young in 1800 [3]. The phenomenon was rediscovered by Coanda in about 1910 and has since been referred to as the 'Coanda Effect'. Wilson and Goldstein [4] investigated the effects of curvature on the development of a turbulent two-dimensional wall jet not immersed in an external flow. They compared the structure and growth of the turbulent boundary layer with results which they, Schwarz and Cosart [5] and Myers et al [6] obtained of a plane boundary layer. They concluded that centrifugal force instabilities introduce rapid mixing of the curved wall jet with its surroundings and cause significant increases in turbulence intensity and Reynolds shear stress in the jet. The increased rate of mixing leads to a greater rate of decay of the maximum velocity in the curved jet than is the case in the plane jet. They noted that the turbulent wall jet boundary was a region of counter gradient shear stress. Novak and Cornelius [7,8] carried out an experimental investigation of the flowfield of an aerofoil with a Coanda jet on the trailing edge with and without external flow using an LDV. It was found that the external freestream plays an important role in the overall mixing and velocity field structure and hence in the growth of the turbulent boundary layer. They together with Launder and Rodi [9] amongst others showed that the existence of a region of counter gradient shear stress is supported by the fact that the position of zero shear stress does not coincide with the position of maximum velocity and that it lies closer to the wall than is the case for a plane surface. Hence, in the case of a curved boundary layer the distribution of shear stress is more significant in the generation of turbulence than is the case in flat plates. Dvorak [10] identified two distinct regions in a turbulent jet on a curved surface which influence its behaviour. In the inner region which is close to the wall the flow behaves like a boundary layer in which deviations from the flow over a flat plate may be attributed to centrifugal effects. The counter gradient shear stress and turbulence production takes place in the outer region and the physical processes taking place in this region dominate the behaviour of the boundary layer.

Wilson and Goldstein [4] as well as Novak and Cornelius [7,8] showed that turbulence intensity in a direction normal to a convex wall is not self preserving and streamwise turbulence intensity is greater than is the case on a flat plate. This suggests that the mechanism of turbulence production through centrifugal force is not as important as that of streamwise turbulence production through the shear mechanism which emerges as the dominant mechanism promoting boundary layer growth.

Various authors including Wilson and Goldstein [4], Wood [11], Raghaven et al [12] and Pulliam et al [13] have shown that the flow in a number of distinct regions influence the performance of a typical circulation control aerofoil. These include i) flow directly upstream of blowing slots, ii) flow being entrained in the wall jet through a jet-shear layer, and iii) development of the wall jet downstream of blowing slots and its ultimate separation from the surface.

Lockwood [14] carried out an experimental investigation of the lift and drag acting on a circulation controlled cylinder with a diameter of 152.4 mm and 8 slots with widths of 0.152 mm distributed evenly around the circumference of the cylinder. The slot distribution could be varied by closing off selected slots and by rotating the cylinder about its axis. The fineness ratio of the cylinder which was fitted with end plates was 8. External flow speeds were typical of those found in the wake of a hovering helicopter rotor with a maximum Reynolds number of 415000 at slot momentum coefficients varying from 0 to 6. Slot distributions tested varied from small angular distributions to those over 360 deg. It was found that the aerodynamic performance of the cylinder was virtually independent of the Reynolds number when blowing was applied. Lift and drag are strongly influenced by slot position for slot configurations covering less than half the cylinder circumference and for such configurations the location of the trailing slot was important.

When slots were equally spaced around the cylinder the lift was low and relatively independent of slot position. Lockwood used a combination of high circulation controlled air pressure and narrow slots while for the results presented here comparatively low static pressures were combined with wider slots.

The 2D experimental work mentioned above provided essential understanding of turbulent boundary layers on a Coanda surface. The experiments did not however include effects found in the wake of a hovering rotor such as i) velocity variations associated with rotor blades that are not fully twisted, ii) those of the trailing vortices, iii) the angular velocity due to the main rotor torque, and iv) time dependent pressure and velocity fields.

Logan and Niji [1,2] describe experiments used to determine the performance of a circulation controlled tail boom located in the downwash of an OH-6A helicopter rotor. The tests simulated in- and out-of-ground effect using one slot. Parameter variations included blade collective pitches up to 10 deg, jet velocities of 36.6 to 68 m/s, slot widths from 4.3 mm to 19 mm and slot angular positions of 90 deg to 150 deg from the 'leading edge' of the cylinder. Harvey [15] reports that it was necessary to add fences to a tail boom fitted with one slot to reduce translational flow along the tail boom to increase its effectiveness. Van Horn [16] carried out tests in a water tank to study the flow interaction at the juncture of the tail boom and fuselage. It was shown that premature separation of the flow from the boom could be prevented by the addition of a second slot to the tail boom at 70 deg from the 'leading edge'.

Until about 1983 computational analyses of circulation controlled aerofoils were based on weakly coupled viscous-inviscid methods [17,18,19]. Morger and Clark [20] describe the use of the low order panel method code VSAERO to analyse the flowfield around a circulation controlled helicopter tail boom. Since ca 1985 Navier-Stokes methods have been used [21,22,23]. In 1989 Shrewsbury [24] compared numerical results obtained using fully explicit Navier-Stokes equations in two-dimensional planar co-ordinates with the experimental results obtained by Novak and Cornelius [7]. The code was executed on the Lockheed/ASG Cray X-MP/24 computer and required 1000 iterations to converge.

Various authors including Dvorak [10] and Pulliam et al [13] amongst others have published modified turbulence models for flow over a curved surface.

2. THEORETICAL BACKGROUND TO COMPUTATIONAL MODEL

Pressure and temperature variations in the flowfield of interest are sufficiently small to neglect compressibility and buoyancy effects. The set of governing equations is comprised of the conservation of mass and momentum plus two additional equations to describe the turbulent kinetic energy and the isotropic dissipation function for turbulence modelling. Using the the two equation k-ε turbulence model [25] the governing set of equations is

$$U_{i,j} = 0 \quad (1)$$

$$\rho \left[\frac{\partial U_j}{\partial t} + U_j U_{i,j} \right] = -p_{,j} + \rho f_i + \left[\mu (U_{i,j} + U_{j,i}) \right]_{,j} \quad (2)$$

for conservation of mass and momentum respectively

$$\rho \left[\frac{\partial k}{\partial t} + U_j k_{,j} \right] = \left[\frac{\mu_t}{\sigma k} k_{,j} \right]_{,j} + \mu_t \phi - \rho \epsilon \quad (3)$$

$$\rho \left[\frac{\partial \epsilon}{\partial t} + U_j \epsilon_{,j} \right] = \left[\frac{\mu_t}{\sigma k} \epsilon_{,j} \right]_{,j} + C_1 \frac{\epsilon}{k} \mu_t \phi - \rho C_2 \frac{\epsilon^2}{k} \quad (4)$$

for turbulent kinetic energy and the isotropic dissipation function. Turbulent eddy viscosity takes the form

$$\mu_t = \rho c \mu \frac{k^2}{\varepsilon} \quad (5)$$

where the different constants take values relevant to a particular flow regime. For turbulent flow in a straight channel the constants have the following values [25]:

$$\mu_t = 0.09 ; \quad C_1 = 1.44 \quad \sigma_k = 1.0; \quad C_2 = 1.92; \quad \sigma_\varepsilon = 1.3 \quad (6)$$

The k-ε model presented above has been shown to be valid in regions away from the wall [25]. Use of the model presented in regions close to the wall gives inferior results due to the inability of the model to resolve sharply varying flow variables in regions close to the wall unless a large number of grid points is used. To overcome this problem a van Driest mixing length model approach is used to model eddy viscosity in regions close to the wall.

In this approach the k-ε model is solved down to the last layer of elements adjacent to the wall where Van Driest's mixing length model is used to resolve turbulent diffusivities of momentum and mass. In this layer of elements special shape functions computed from universal flow profiles (Couette flow) are used. The near wall region consists of the well known laminar viscous sublayer, the transition or buffer region and the fully turbulent region as shown in figure 1.

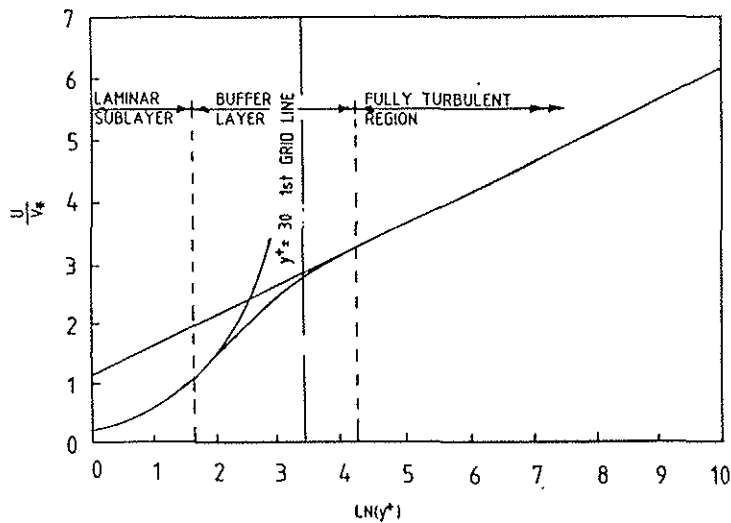


Figure 1 Structure of Boundary layer

The turbulent eddy viscosity over the last layer of elements is given by

$$\mu_t = \rho l_m^2 [(U_{i,j} + U_{j,i}) U_{i,j}]^2 \quad (7)$$

where l_m is the van Driest mixing length defined as [25]:

$$l_m = \kappa \delta \left[1.0 - e^{-\frac{y^+}{A}} \right] \quad (8)$$

2.1 Computational Grid and Boundary Conditions

The computational grid over the entire domain is presented in figure 2. It was developed on a trial-and-error basis to ensure that the layer of elements adjacent to solid boundaries corresponded to the thickness of the near wall region as computed from Couette profiles. This thickness corresponds to $y^+ = 30$ throughout the computational domain. This ensures accurate modelling of the near wall region viscosity and computation of turbulence development and growth through the boundary layer.

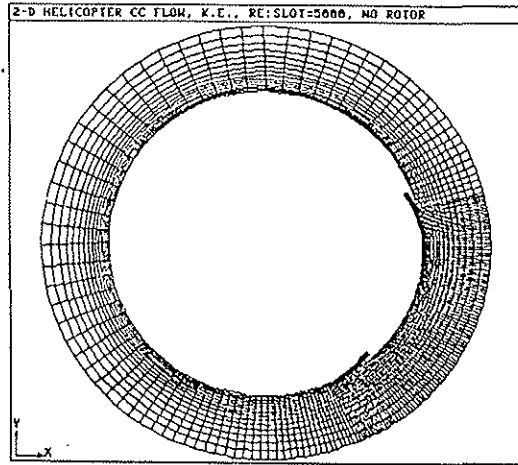


Figure 2 Computational Grid

The computational mesh was comprised of 1390 elements. The governing equations were discretised using the linear finite element basis using four noded elements throughout the computational domain.

Boundary conditions used on solid and far field boundaries are standard as defined in reference 25. The no-slip boundary condition of zero tangential and normal velocity was enforced on all solid boundaries. A parabolic velocity distribution, typical of a laminar flow profile, was specified at the blowing slot origin. The distribution was specified in terms of normal velocity components (i.e. parallel to the direction of the blowing slot) with radial velocity components being constrained to zero. Far field boundary conditions were not constrained for the analyses in which the downwash was zero.

Appropriate boundary conditions are needed at the interface between the layer of elements directly adjacent to solid boundaries and the rest of the domain, as transition between the k - ϵ and van Driest mixing length turbulence models take place here. Turbulent kinetic energy is assumed constant over the wall region so that the Neumann boundary condition

$$\frac{\partial k}{\partial n} = 0 \quad (9)$$

at the interface applies. Close to wall the turbulence length scale defined as $k^{1.5/\epsilon}$ varies linearly with normal distance from the wall. The Dirichlet boundary condition for ϵ at the interface is then:

$$\epsilon = \frac{(C_{\mu} k)^{1.5}}{k \delta} \quad (10)$$

3. EXPERIMENTAL EQUIPMENT

The rig, shown in figure 3, is comprised of a rotor test facility [26] to which a circulation controlled tail boom has been added [27]. The flow in the boundary layer on the tail boom was measured using a combination of yaw, Pitot and Prandtl static pressure probes. These probes may be moved by means of a computer controlled traversing mechanism shown in figure 4.

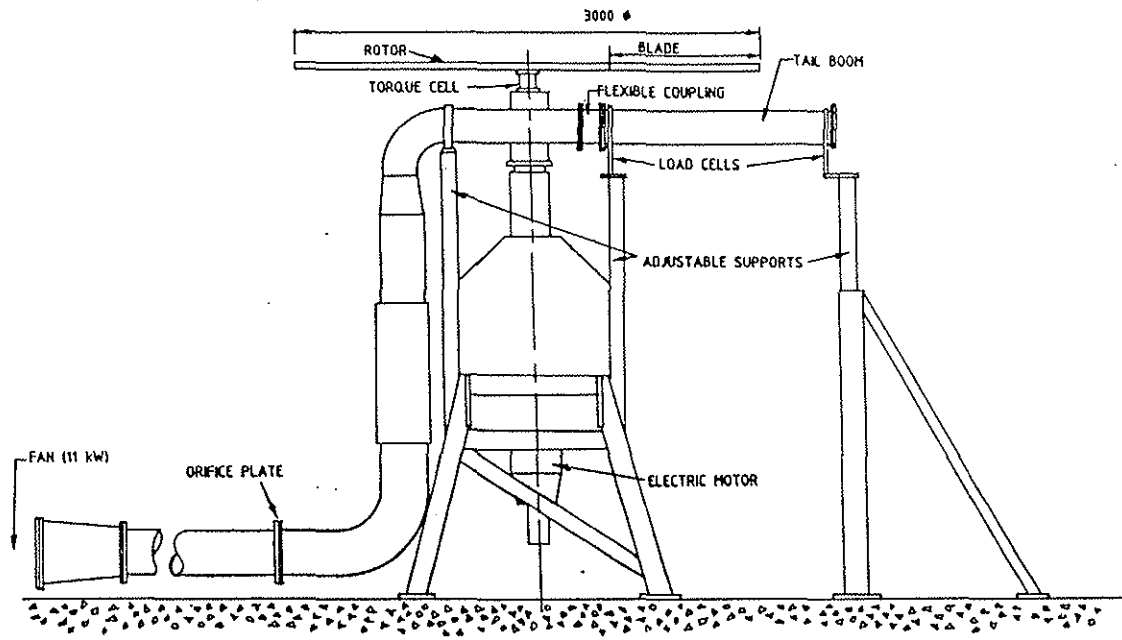


Figure 3 General Arrangement of Test Rig

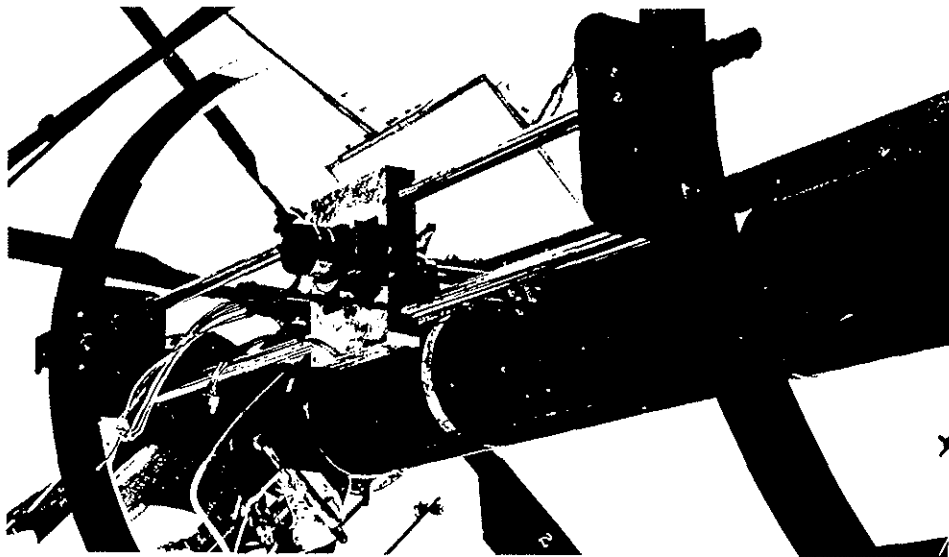


Figure 4 Probe Traversing Mechanism

Parameters which may be measured on the rotor test facility include mean values of the rotor thrust, speed and torque. The blade collective pitch is set manually. The rotor has five untwisted blades with a diameter of 3.0 m and a constant chord of 0,191 m.

The tail boom is supported on load cells at each end of the boom which can measure forces normal and parallel to the rotor disc plane. A cross-section of the tail boom is shown in figure 5. The slot width is maintained constant with spacers which also add to the rigidity of the composites cylinder. The distance of the boom from the rotor disc plane is adjustable.

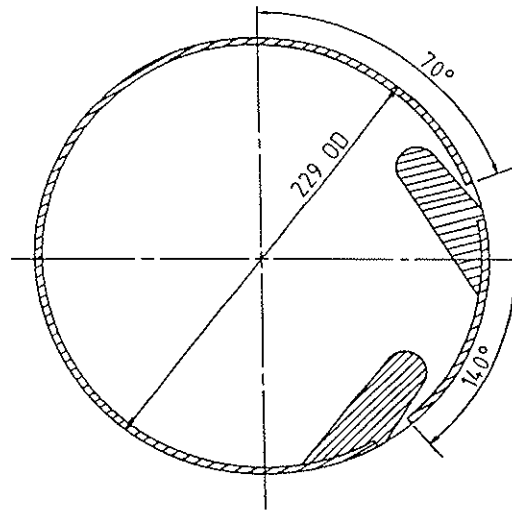


Figure 5 Cross-Section of Tail Boom

Air is supplied to the tail boom by means of a fan located on the ground. Air flow to the tail boom is measured by means of an orifice plate designed according to BS 1042. The static pressure in the tail boom is measured at the the tail boom. The thruster was removed for this series of tests to avoid masking torque effects due solely to circulation control. The ranges and standard deviations of the transducers are given in table 1.

Table 1 Range and Standard Deviations of Transducers

| COMPONENT | RANGE | STANDARD DEVIATION (% OF FULL SCALE) |
|-----------------------------------|-------|---|
| Rotational Speed (rev/min) | 2000 | .25 |
| Rotor Thrust (N) | 5000 | .82 |
| Rotor Torque (Nm) | 380 | .48 |
| Boom Load Cells (N) | 100 | 0.39 |
| Boom Pressure (N/m ²) | 5000 | 0.25 |

All readings were collected under computer control. Zero readings were taken for each transducer prior to the commencement of a test and all parameters are measured relative to the zero reading. Each data point was averaged from 20 readings with each data set being taken at one second intervals.

4. EXPERIMENTAL PROCEDURE

4.1 Velocity Measurements In The Boundary Layer

For each set of readings the flow angle was measured using a two hole yaw probe. The total and static pressures were then measured by means of a Prandtl total head tube and a static pressure probe relative to a point in the atmosphere which was far removed from the rotor. Care was taken to ensure that the total head and static pressures were measured at the same point to eliminate the effects of pressure gradients in the direction of flow.

4.2 Torque Due to Circulation Control Air

With the rotor stationary the boom torque was measured at various static pressures in the tail boom with various slot lengths. The length of both slots was similar for each test. The static pressure in the boom was varied by throttling the air to the fan.

4.3 Boom Torque Due to Rotor Torque

With no air flow to the tail boom the boom torque was measured at various rotor speeds. Tests were carried out with combinations of collective pitch settings of 10, 15 and 20 deg and distances of the boom centreline of 430 mm and 747 mm below the rotor disc plane.

4.4 Torque Due to Combined Effects of Circulation Control and Rotor Downwash

For each test the collective pitch, boom static pressure and distance of the boom below the rotor disc was set and the rotor speed was varied.

5. ANALYSIS OF EXPERIMENTAL RESULTS

5.1 Torque Due to Circulation Control

The flow of the air on the surface of the tail boom after it has exited from the slots and the region where the flow leaves the surface of the tail boom is a boundary layer problem. The purpose of the experiments was to quantify the effects of the boom pressure on the tail boom torque in general and for the configuration tested in particular.

The force, per unit length acting on the tail boom in a direction parallel to the rotor disc will be a function of the momentum of the air in the boundary layer, the structure of the boundary layer and the angular point at which it leaves the tail boom. As the axial velocity of the air in the tail boom is small compared to its exit velocity the flow from the tail boom is essentially constant along its length [30]. The force per unit boom length can then be related the static pressure of the air in the tail boom, the total slot thickness, the boom radius, the air density and the viscosity of the air. Using dimensional analysis to obtain the flow per unit boom length and integrating the result with respect to slot length gives

$$Q = K(L_2^2 - L_1^2) P R_b \left(\frac{\mu^2}{P \rho R_b^2} \right)^a \left(\frac{t}{R_b} \right)^b \quad (10)$$

where K, a and b are constants for a particular geometry. The term $\left(\frac{\mu^2}{P \rho R_b^2} \right)^{\frac{1}{2}}$ is a Reynolds number.

The range of variables for the tests carried out are presented in table 2.

Table 2 Domain of Tests for Boom Torque Due to Jets Only

| TEST NO | P_{min} (N/m ²) | P_{max} (N/m ²) | $(L_2^2 - L_1^2)$ (m ²) |
|---------|----------------------------------|----------------------------------|--|
| 293 | 950 | 2740 | 3.654 |
| 294 | 815 | 2990 | 2.900 |
| 295 | 1230 | 3240 | 2.194 |
| 296 | 1210 | 3420 | 1.646 |
| 297 | 2050 | 3580 | 1.130 |

It was found that the boom torque is not dependent on the Reynolds number and hence a=0. The results for the geometry tested are presented in figure 6.

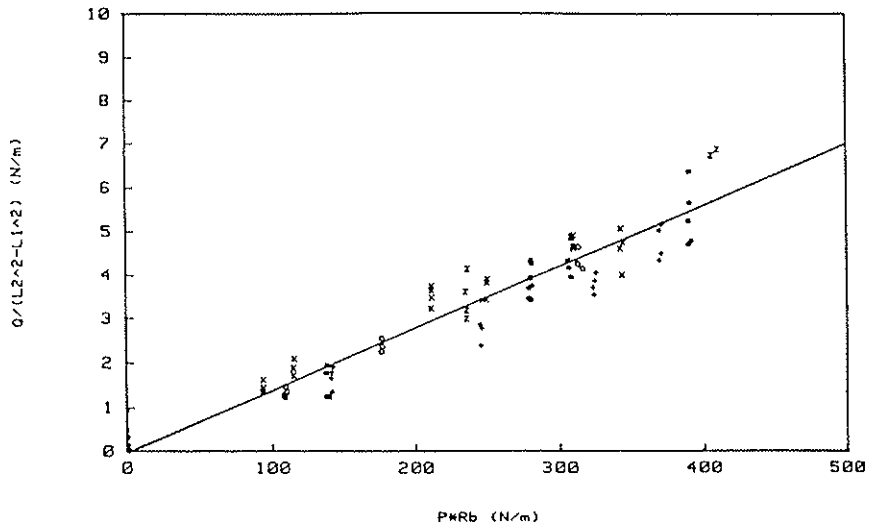


Figure 6 Variation of $Q/(L_2^2 - L_1^2)$ with PR_b

A linear regression of the results resulted in

$$Q/(L_2^2 - L_1^2) = -0.234 + 0.01461 PR_b \quad (11)$$

For the geometry tested

$$Q = 0.00160 (L_2^2 - L_1^2) P \quad (12)$$

with a coefficient of correlation of 0.937. This component of the boom torque acts in a direction which counteracts that applied to the main rotor.

5.2 Boom Torque Due to Rotor Torque

For the case of no circulation control air the combined effects of the time dependent pressure, angular and axial velocities of the air in the rotor wake result in a component of the torque acting on the tail boom in the same direction as that applied to the main rotor. It was found that this component of the boom torque is proportional to the main rotor torque as shown by a typical set of results presented in figure 7.

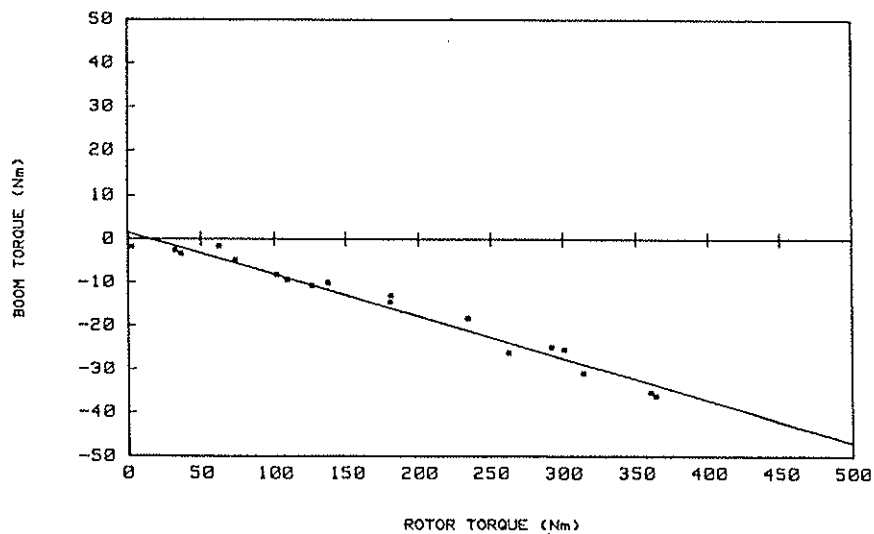


Figure 7 Variation of Boom Torque with Rotor Torque.

If it can be assumed that the tail boom torque is a function of the rotor torque, air density and viscosity, rotor radius, boom diameter and distance of the tail boom below the rotor then it may be shown that

$$Q = K \frac{\mu^2 R_r}{\rho} \left(\frac{Q_r \rho}{\mu^2 R_r} \right)^a \left(\frac{R_b}{R_r} \right)^b \left(\frac{H}{R_r} \right)^c \quad (13)$$

For the data available Q is proportional to Q_r and hence $a = 1$. It also appears that over the range of H tested that Q is independent of H and hence $c = 0$. For the particular geometry tested equation (13) may be written

$$Q = K Q_r \quad (14)$$

Values of dQ/dQ_r obtained for tests carried out are presented in figure 8.

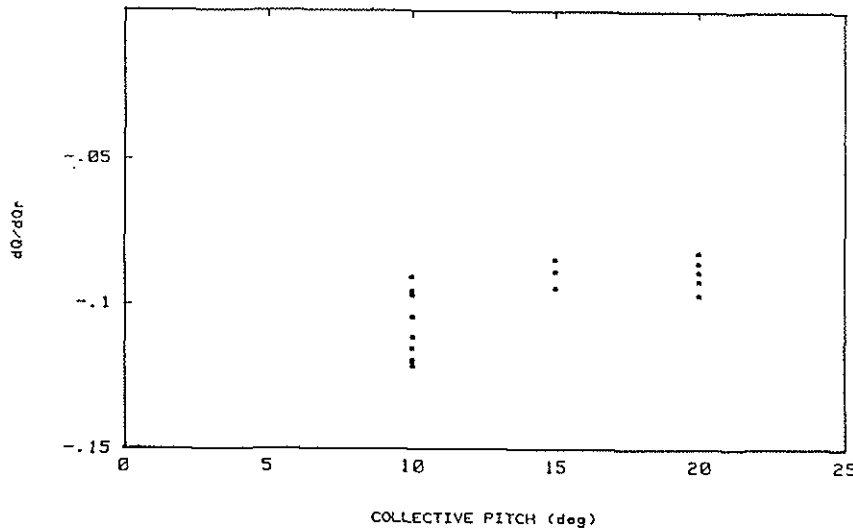


Figure 8 Variation of dQ/Q_r with Collective Pitch

The scatter in the experimental results may be attributed to the low boom torques. While it appears that the ratio of the boom to the rotor torque is a function of the blade collective pitch no attempt has been made, due to the scatter to relate the boom torque performance to any relevant parameters. A mean value for dQ/dQ_r of -0.0972 with a standard deviation of 0.01125 was calculated for the available data.

$$Q = -0.09772 Q_r \quad (15)$$

5.3 Torque Due to Combined Effects of Circulation Control and Rotor Downwash

Any description of the tail boom torque developed by the combined effects of the rotor downwash and the circulation generated by the air jets must include the case where there is either no downwash or no circulation control air.

If for a given system geometry the boom torque due to the combined effects of rotor downwash and circulation control only is a function of the rotor thrust (mean downwash velocity), rotor radius, boom pressure (jet velocity), slot thickness, boom diameter and air density and viscosity then it may be shown that

$$\frac{Q}{T R_b} = K \left(\frac{P R_b^2}{T} \right)^a \left(\frac{\rho P R_r^2}{\mu^2} \right)^b \left(\frac{R_b}{R_r} \right)^c \left(\frac{t}{R_r} \right)^d \quad (16)$$

which for a given geometry may be written

$$\frac{Q}{T R_b} = K \left(\frac{P R_b^2}{T} \right)^a \left(\frac{\rho P R_r^2}{\mu^2} \right)^b \quad (17)$$

From the experimental data it was established that the boom torque is proportional to the rotor thrust, hence $a = 0$, and to the square root of the boom static pressure. Thus for the given geometry, if the effects of circulation air and rotor torque are included then

$$Q = 0.00160 (L_2^2 - L_1^2) P - 0.09772 Q_r + 0.001691 T P^{\frac{1}{2}} \quad (18)$$

The coefficient 0.001691 was obtained by correlating

$$J = (Q - 0.00160 (L_2^2 - L_1^2) P + 0.0977 Q_r) / P^{\frac{1}{2}} \text{ with the rotor thrust for 38 tests.} \quad (19)$$

The results from 10 tests are plotted in figure 9.

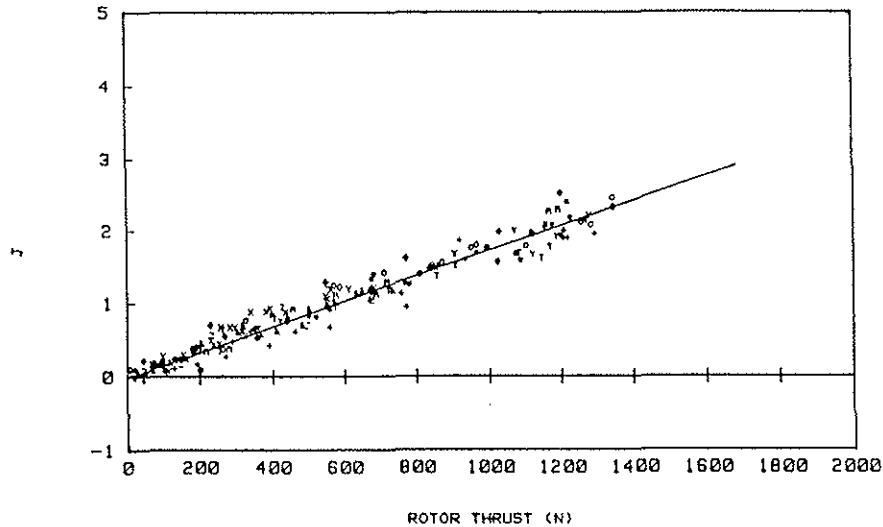


Figure 9 Variation of J with Rotor Thrust

6. COMPUTATIONAL RESULTS

Computational models were validated against experimental results obtained with a slot Reynolds number of 5000.

The present $k-\epsilon$ model constants were fine tuned over a range of experimental results for the present blowing slot configuration to obtain good correlation between experimental and computational velocity profiles for the case of no downwash. The new set of constants are

$$\mu_t = 0,09; C_1 = 1,309; \sigma_k = 1,0; C_2 = 2,112; \sigma_t = 1,3 \quad (20)$$

In figure 10 a typical comparison between a measured experimental and computed wall jet velocity profile downstream of the upper blowing slot. The angular position of flow separation was correctly predicted to within 5%. The torque acting on the tail boom in a plane parallel to the rotor disc was determined for the case of no downwash and a boom pressure of 3100 Pa using the computational model. The computed torque was 17,31 N which compares favourably with a torque of 18,2 N obtained using equation (12).

Figure 11 presents computed velocity vectors for the case of no rotor downwash. Evident from the velocity vector plot is the rapid development of the characteristic turbulent velocity profile in the blowing slot so that turbulent flow is fully developed by the time the slot exit is reached.

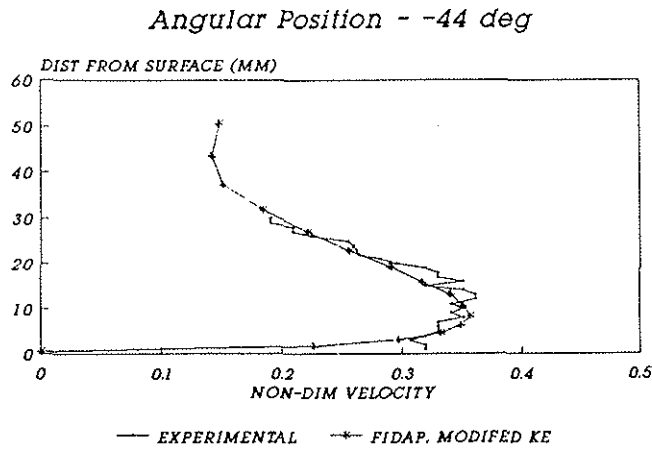


Figure 10 Comparison of Computational and Experimental Velocity Profiles

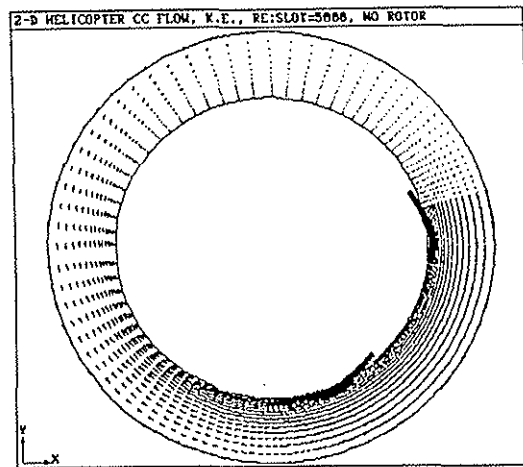


Figure 11 Computed Velocity Vector Field

This growth trend can be attributed to the viscous shear mechanism present in the fluid between the upper part of the boundary layer and the edge of the wall jet. Computed pressure contours for the configuration are presented in figure 12. Comparison of the computed pressure contours for the curved wall jet configuration with those computed for straight wall jets show the curved wall pressure contours not to be as widely distributed through the boundary layer as is the case for the straight wall jet configuration [30].

The present computational model predicts an entirely unstable region of turbulence production for the outer boundary or mixing layer as is evident from the computed turbulent kinetic energy contours presented in figure 13. Comparison of the computed velocity vector field with the turbulent kinetic energy contours shows regions of high turbulent kinetic energy gradients to be coincident with regions of maximum velocity. This promotes turbulence production and hence boundary layer growth.

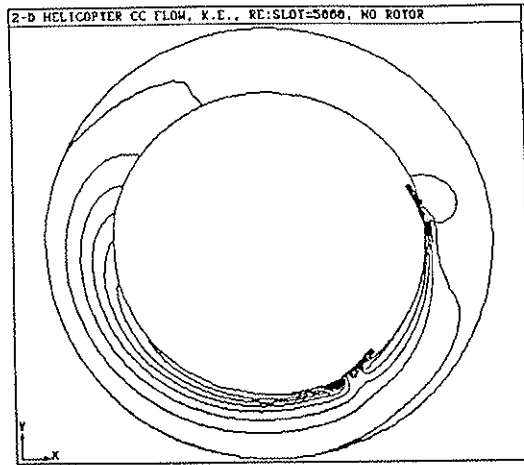


Figure 12 Computed Pressure Contours

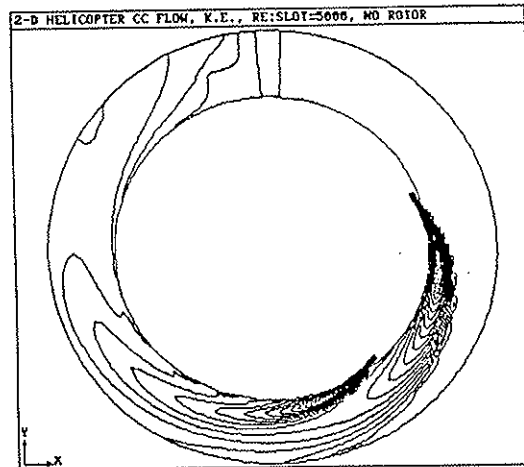


Figure 13 Computed Turbulent Kinetic Energy Contours

7. CONCLUSIONS

7.1 Experimental Work

The torque developed by a circulation controlled cylindrical helicopter tail boom in the downwash of a hovering rotor about the rotor axis is comprised of three components.

The effect of the air pressure in the boom alone is to cause air to flow out through the jet slots and due to the Coanda effect this air remains attached to the cylinder and leaves the cylinder at a point on the 'opposite' side of the cylinder to the slots. This results in a torque which acts in a direction which counterbalances that applied to the main rotor. For a given geometry and for the range of boom pressures tested the torque is proportional to the static pressure of the air in the boom.

In the absence of circulation control air the velocity and pressure fields in the rotor wake produce a torque on the tail boom which for a given geometry is proportional to the rotor torque.

The combined effects of the rotor downwash and circulation control air generates a torque component which is approximately an order of magnitude greater than that of either the two components mentioned above. For a given geometry this component of torque is proportional to the rotor thrust and the square root of the gauge pressure of the air in the tail boom.

7.2 Computational Work

The jet boundary layer consists of two distinct regions. Growth of the inner boundary layer ($y^+ \approx \leq 30$) is well predicted by using a van Driest mixing length model in this region, and shows excellent correlation with experimental results.

The outer boundary layer ($y^+ \approx \geq 30$) has been shown to be a region of counter gradient shear stress. This region is primarily responsible for mass flow entrainment and turbulence propagation through the mechanism of shear gradients in the fluid.

The correct prediction of these shear gradients in the fluid is essential in predicting the ultimate performance of the wall jet. The current turbulence model constants were modified by $\approx 10\%$ to obtain good correlation between computed and experimental results.

The results of the present work suggests that the development and growth of a turbulent wall jet over a curved surface is primarily governed by viscous shear mechanisms present in the outer boundary layer.

For the case of no downwash the torque calculated using the computational method agrees with that measured to within 5%.

8. REFERENCES

- [1] Logan A H **Experimental Investigation of a Circulation Control Boom Under a Statically Thrusting OH-6A Main Rotor** Hughes helicopters Inc., HH78-29, 1976
- [2] Logan A H and Niji K K **Experimental Investigation of a Circulation Control Tail Boom Under a Statically Thrusting OH-6A Main Rotor** Hughes Helicopter Report 150-A-2001, February 1976
- [3] Young T **Outlines of Experiments and Inquiries Respecting Sound and Light** Lecture to Royal Society, 16 January 1800.
- [4] Wilson D J and Goldstein R J **Turbulent Wall Jets with Cylindrical Streamwise Surface Curvature** *Journal of Fluids Engineering*, Vol. 96, 1976, pp. 550-557
- [5] Schwarz W H and Cosart W P **The Two-Dimensional Turbulent Wall Jet** *Jour. of Fluid Mech.*, Vol. 10, Pt4, 1961, p481
- [6] Myers G E, Schauer J and Eustis R H **Plane Turbulent Wall Jet Flow Development and Friction Factor** *Jour. Basic Eng. Trans. ASME, Series D*, Vol. 85, 1963, p.47
- [7] Novak C J and Cornelius K C **An LDV Investigation of a Circulation Control Airfoil Flowfield** AIAA Paper No. 86-0503, 1986
- [8] Novak C J and Cornelius K C **Investigations of a Circulation Control Flowfield Using an Advanced Laser Velocimeter** Circulation Control Workshop, NASA CR 2430, 1986
- [9] Launder B A and Rodi W **The Turbulent Wall Jet - Measurements and Modelling** *Annual Rev., Fluid Mechanics*, 1983
- [10] Dvorak F A **Calculation of Turbulent Boundary Layers and Wall Jets Over Curved Surfaces** AIAA Journal, Vol 11, No 4, April 1973

- [11] Wood N J **The Further Development of Circulation Control Airfoils** Circulation Control Workshop, NASA CR 2430, 1986
- [12] Raghaven V, Chopra I and Rai S **Circulation Control Airfoils in Unsteady Flow** Journal of the American helicopter Society, October 1988
- [13] Pulliam T H, Jespersen D C and Barth T J **Navier Stokes Computations for Circulation Control Airfoils** Circulation Control Workshop, NASA CR 2430, 1986
- [14] Lockwood V E **Lift Generation on a Circular Cylinder by Tangential Blowing From Surface Slots** NASA Technical Note D-244, May 1960, 38p
- [15] Hanvey S A **NOTAR - No Tail Rotor (Circulation Control Tail Boom)** 26 Annual Symposium of the Society of Experimental Test Pilots, 25 September 1982
- [16] Van Horn J R **NOTAR (No Tail Rotor) Hover Testing Using a Scale Model in Water** 42nd Annual Forum of the American Helicopter Society, Washington, D.C., June 2-4, 1986
- [17] Gibbs E H and Ness **Analysis of Circulation Controlled Airfoils** Dept. Aerospace Engineering, West Virginia University, Rept TR-43, June 1975
- [18] Dvorak F A and Kind R J **Analysis Method for Viscous Flow over Circulation Controlled Airfoils** J. of Aircraft, Vol. 16, January 1979
- [19] Dvorak F A and Choi D H **Analysis of Circulation Controlled Airfoils in Transonic Flow** AIAA J. of Aircraft, Vol. 20, No. 4, April 1983
- [20] Morger K M and Clark D R **Analytic and Experimental Verification of the NOTAR Circulation Control Boom** 40th Annual Forum of the American Helicopter Society, Arlington, Virginia, May 1984, pp. 419-428
- [21] Berman H A **A Navier-Stokes Investigation of a Circulation Control Airfoil** AIAA Paper 85-0300, January 1985
- [22] Pulliam T J, Jespersen D C and Bth T **Navier-Stokes Computations for Circulation Controlled Airfoils** AIAA Paper 85-1587, July 1985
- [23] Shrewsbury G D **Numerical Evaluation of Circulation Control Airfoil Performance Using Navier-Stokes Methods** AIAA Paper 86-0286, January 1986
- [24] Shrewsbury G D **Numerical Study of A Research Circulation Control Airfoil Using Navier-Stokes Methods** J. of Aircraft, Vol. 26, No. 1, January 1989
- [25] Fluid Dynamics International **Introduction Theoretical FICONV System** Fluid Dynamics Analysis Package, Release 5.02, 1990
- [26] Nurick A, Green W and Poprawa S A H **Commissioning of a Helicopter Rotor Test Facility** Research Report No. 86, School of Mechanical Engineering, University of the Witwatersrand, October 1985
- [27] Nurick A and Fonternei M A **Commissioning of a Helicopter Tail Boom Circulation Control Test Rig** Research Report No. 92, School of Mechanical Engineering, University of the Witwatersrand, July 1990
- [28] Janakiram R D and Hassan A A **Rotorcraft Computational Fluid Dynamics - Recent Developments at McDonnell Douglas** Paper 16, Fourteenth European Rotorcraft Forum, Milano, Italy, 20-23 September 1988
- [29] Groesbeek C and Nurick A **Modelling of a Helicopter Circulation Control Tail Boom using a 2D Navier Stokes Code** 3rd South African Aeronautical Engineering Conference, Pretoria, July 1991
- [30] Groesbeek C **Analysis of Flow on a Circulation Controlled Helicopter Tail Boom** MSc Dissertation, University of the Witwatersrand, 1992